



Acidic corrosion of mild steel in the presence of acetic acid: Mechanism and prediction



Aria Kahyarian^{*}, Alex Schumaker, Bruce Brown, Srdjan Nesic

Institute for Corrosion and Multiphase Flow Technology, Department of Chemical and Biomedical Engineering, Ohio University, Athens, OH, 45701, USA

ARTICLE INFO

Article history:

Received 22 September 2017
 Received in revised form
 12 November 2017
 Accepted 15 November 2017
 Available online 26 November 2017

Keywords:

Corrosion
 Acidic
 Mild steel
 Acetic acid
 Mechanism

ABSTRACT

The mechanism and the kinetics of mild steel corrosion in deaerated aqueous acetic acid solutions was investigated. The behavior of the steady state voltammograms, obtained at pH 3 to pH 5 and acetic acid concentrations up to 41.5 mM, showed that the direct reduction of undissociated acetic acid is not significant, in contrast to what is commonly reported in the literature. Nevertheless, acetic acid was shown to influence the corrosion process, first by increasing the cathodic limiting current through buffering the hydrogen ion concentration at the metal surface, and second by inhibiting the rates of both anodic and cathodic charge transfer reactions by chemically adsorbing onto the metal surface. Considering these mechanistic observations, a comprehensive mathematical model was developed and verified, using the experimental results. The counterpoising effect of acetic acid on the limiting current and the rate of electrochemical reactions was shown to be able to justify the inconsistent and sometimes contradictory behavior previously reported in the literature. Additionally, increasing the temperature was shown to have a synergistic effect with acetic acid concentration on the observed corrosion rates. This behavior is a result of shifting corrosion currents towards the mass transfer controlled range at elevated temperatures, where acetic acid has a determinant effect.

© 2017 Elsevier Ltd. All rights reserved.

1. Introduction

Besides carbon dioxide (CO₂) and hydrogen sulfide (H₂S), short chain organic acids such as formic acid (CHOOH), acetic acid (CH₃COOH), and propionic acid (CH₃CH₂COOH) are amongst the common corrosive species encountered in the oil and gas industry [1–5]. Organic acids are commonly reported to be present in the co-produce aqueous phase with concentrations up to several hundred milligrams per liter [6–9]. Amongst the organic acids, acetic acid (HAc in short) is the most abundant species [6,7,9,10], which has been commonly used to represent the effect of all organic acids in corrosion studies, at least as far as it concerns the oil and gas industry.

Reports on the significance of organic acids in corrosion of pipeline steel can be found as early as the 1940s [11], however, the subject gained little attention until 1980's. To date, there seems to be a consensus on the significance of acetic acid in corrosion of mild steel, however, the reported effect of acetic acid on the observed

corrosion rates in the literature appears inconsistent or even contradictory in some cases, as discussed in the following.

Numerous research studies have focused on elucidating the corrosion mechanisms related to the presence of acetic acid in oil and gas transmission pipelines. Gulbrandsen and Bilkova [12] studied the effect of acetic acid on CO₂ corrosion of X65 mild steel. The authors reported mixed behavior of corrosion rates at low and high temperatures as the concentration of acetic acid was increased. Based on their observations at 25 °C, corrosion rates decreased with increasing acetic acid concentrations, whereas the opposite behavior was reported at 80 °C. This was justified based on observation of an inhibitive effect of acetic acid on the anodic reaction. The authors argued that the combination of anodic reaction retardation and increase in cathodic reaction rate, as a result of direct acetic acid reduction, leads to this mixed behavior. In 2007, George and Nesic [13] investigated the effect of acetic acid on aqueous X65 mild steel corrosion under CO₂ and N₂ atmospheres in controlled pH experiments. The reported corrosion rates at pH 4, with or without CO₂ present, showed a significant increase with addition of a 100 ppm (1.66 mM) acetic acid, whereas further increase of acetic acid concentration to 1000 ppm (16.6 mM) did not result in significantly higher corrosion rates. The authors also

^{*} Corresponding author.

E-mail address: ak702711@ohio.edu (A. Kahyarian).

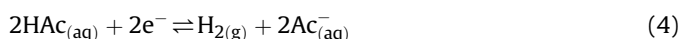
reported that as temperature was increased to 40 °C and 60 °C, the addition of 100 ppm acetic acid had a more pronounced effect on increasing the corrosion rates. The increased corrosion rates in the presence of acetic acid was associated with the direct acetic acid reduction during the corrosion process. The authors also confirmed the previous reports of a slight inhibitive effect of acetic acid on the iron dissolution reaction. Using a similar approach as George and Nescic [13], Okafor et al. [14] studied the effect of acetic acid at temperatures up to 80 °C and acetic acid concentrations up to 5000 ppm. It was reported that increasing the acetic acid concentration resulted in higher corrosion rates at all the studied conditions. The increased corrosion rates were justified by the direct reduction of acetic acid, which was claimed to be supported by a higher activation energy obtained for cathodic reactions when acetic acid was present. However, the reported cathodic polarization curves in that study appear to be significantly influenced by the limiting current almost in all conditions, hence, the electrochemical activation energies could not be obtained with reasonable confidence. In 2012, Jia et al. studied the effect of acetic acid in CO₂ corrosion of 3Cr low-alloy steel [15], reporting a significant increase of corrosion rates by increasing the total acetic acid concentration from 0 to 2000 ppm. The author associated the higher corrosion rates with the direct reduction of acetic acid as well as its effect on degrading the protective corrosion product layer. Nevertheless, the arguments used to justify the observed behavior could be questioned when considering the lack of proper solution speciation control in their experiments. One should consider that increasing the acetic acid concentration from 0 to 2000 ppm could decrease the solution pH dramatically; a key factor when discussing the corrosion behavior which was not included in analysis of data in that study [15]. Zhu et al. [16] also studied the CO₂ corrosion of N80 carbon steel in acetic acid containing solutions with emphasis on elevated temperatures and CO₂ partial pressures. A significant increase of corrosion rates with increasing acetic acid concentrations at 90 °C was reported, which were justified by similar arguments used by Jia et al. [15].

Considering the brief review above, the increased corrosion rates in the presence of acetic acid were commonly justified by presuming that acetic acid is directly reduced at the metal surface. According to this mechanistic view, as a weak acid, acetic acid is only partially dissociated in the aqueous phase (Reaction (1)). Hence, both acetate ions (Ac⁻) and undissociated acetic acid

(molecular HAC) are present in an aqueous solution, while their relative concentrations are defined by the solution pH (Fig. 1).



In this corrosion mechanism, the anodic iron dissolution (Reaction (2)) is accompanied by two parallel cathodic reactions, namely, hydrogen ion reduction (Reaction (3)) and the direct reduction of the undissociated acetic acid (Reaction (4)).



However, in more recent years, evidence has been mounting that suggests acetic acid is not a significant electroactive species and its sole contribution to the cathodic currents is through the homogeneous Reaction (1). In this mechanistic view, acetic acid merely acts as a hydrogen ion carrier in the solution and its presence would only increase the mass transfer limit of the cathodic currents. This mechanism points to the fact that at mass transfer limiting current, where the surface pH is increased, the chemical equilibrium of acetic acid (Reaction (1)) shifts towards acetic acid dissociation, therefore, acetic acid acts as an additional source of hydrogen atoms at the metal surface. In 2011, Amri et al. [17] studied the effect of acetic acid in CO₂ corrosion in the context of top of the line corrosion of X65 mild steel. The authors reported that when the corrosion current was controlled by the electrochemical reaction rates (as opposed to mass transfer limited) at lower pH values, increasing the acetic acid concentration did not significantly affect the observed corrosion rates or the corrosion mechanism. It was reported that the effect of acetic acid was mainly related to increasing the limiting current and that the direct reduction of acetic acid was insignificant. It was also suggested that acetic acid inhibits the anodic reaction and therefore local changes in its surface concentration could trigger localized attack. In another, more systematic study, Tran et al. [18] investigated the behavior of the cathodic polarization curves in mildly acidic environments, with acetic acid being the only weak acid present in solution. The polarization curves were obtained on 304 stainless steel in order to eliminate the interference of anodic reactions on the observed cathodic current. It was explicitly shown that the concentration of acetic acid did not affect the charge transfer controlled portion of the cathodic sweeps. Therefore, the authors concluded that acetic acid is not involved in a charge transfer processes directly, and its main contribution was buffering the surface hydrogen ion concentration, thereby increasing the limiting currents. However, considering the possible influence of the alloying compounds of 304 stainless steel (~20 wt % Cr, and 10 wt % Ni) and the passive layer on the electroactivity of the metal surface, the experimental findings of Tran et al. [18] on stainless steel could not be considered valid for mild steel, without further verification. In 2016, Kahyarian et al. [19] investigated the effect of acetic acid on the polarization behavior of pure iron and X65 mild steel. Based on the experimental data obtained using rotating disk electrodes and potentiodynamic measurements, the authors showed that acetic acid did not significantly contribute to the charge transfer controlled currents for concentrations up to 1000 ppm. Hence, the mechanism proposed by Tran et al. [18] was also proven to be valid for iron and mild steel surfaces.

The present study expands on the experimental conditions covered previously by Kahyarian et al. [19], in order to further

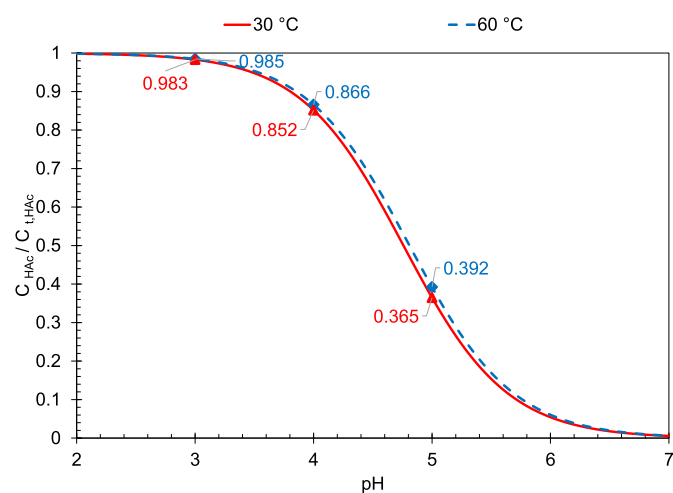


Fig. 1. The ratio of undissociated acetic acid concentration to total acetate species concentration in 0.1 M NaCl solution for various pH values at 30 °C and 60 °C. The labels from left to right show the ratio at pH 3.0, pH 4.0, and pH 5.0.

elucidate the underlying mechanisms of the aqueous mild steel corrosion in the presence of acidic acid. A quantitative analysis of the results, using comprehensive mathematical calculations, is included in the present study, to provide a detailed description of the mechanistic observations. Ultimately, these mathematical relationships can be incorporated into mechanistic corrosion rate predictive models [20,21] for application in more elaborate corrosion scenarios.

2. Materials and methods

2.1. Experimental procedure

The experiments were carried out in a 1 L glass cell with a conventional three electrode arrangement and a silver/silver chloride reference electrode, similar to that described in an earlier study [22]. The supporting electrolyte was 0.1 M solution of sodium chloride in deionized water in all of the reported experiments. The targeted solution composition was achieved by addition of the desired amount of glacial acetic acid followed by adjustment of the solution pH using small amounts of dilute HCl or NaOH solutions. All the chemicals used in the present study were analytical grade. The solution was then purged using nitrogen gas for minimum of 90 min while the oxygen content of the outlet gas was monitored (Orbisphere 410). The maximum allowed dissolved oxygen content before introducing the working electrode into the solution was 1 ppb.

The working rotating disc electrode (RDE) was made of an API 5L X65 mild steel disc (composition given in Table 1) with 5 mm diameter, press-fitted into a Teflon™ electrode holder (Pine instruments). The electrode was abraded with 1000 grit silicon carbide paper and further mirror polished using successively finer silicon suspensions, down to 0.25 μm, prior to each test. The electrode was then rinsed and sonicated in isopropanol for 5 min and dried with nitrogen gas. The working electrode was inserted into the glass cell while the nitrogen gas flow was temporarily increased and further electrochemically treated as described in detail elsewhere [19]. As the last step, the open circuit potential (OCP) was monitored for 10 min prior to electrochemical measurements in order to assure a steady OCP reading (maximum allowed drift of ±2 mV over 5 min).

The polarization curves were obtained using stair case voltammetry with the scan rate of 0.5 mV s⁻¹ and sampling period of 2 s⁻¹. The anodic and cathodic polarization curves were obtained in separate experiments, by sweeping the potentials from OCP towards more positive and more negative potentials, respectively. The reported results were corrected for ohmic drop using the solution resistance obtained from electrochemical impedance spectroscopy (EIS) measurements, performed after polarization measurements. The EIS measurements were conducted at OCP in the frequency range of 0.2 Hz–5 kHz with an AC perturbation potential of ±5 mV.

The reported corrosion rates were obtained from linear polarization resistance (LPR) measurements, conducted in separate experiments, following the abovementioned preparation procedure. For LPR measurements, the potential range of ±5 mV vs. OCP and scan rate of 0.125 mV s⁻¹ was used. The experimental conditions are summarized in Table 2.

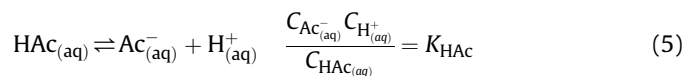
Table 1
Chemical Composition of the X65 Mild Steel in wt%.

S	P	V	C	Cr	Mo	Si	Ni	Mn	Fe
0.009	0.009	0.047	0.13	0.14	0.16	0.26	0.36	1.16	Balance

2.2. Numerical methods and mathematical modeling

2.2.1. Water chemistry calculation

The solution speciation can be obtained considering the chemical equilibria of the involved homogeneous reactions. In an aqueous solution containing acetic acid, the two homogeneous reactions are the acetic acid dissociation shown via Reaction (5) and water dissociation shown via Reaction (6).



The chemical equilibria corresponding to acetic acid and water dissociation can be mathematically expressed as Equation (5) and Equation (6), respectively, using the equilibrium constants listed in Table 3.

Assuming that acetic acid concentration in the gas phase was negligible, the total acetate concentration ($C_{t,\text{HAC}}$) may be related to undissociated acetic acid concentration (C_{HAC}) through a mass balance relationship described as Equation (7).

$$C_{t,\text{HAC}} = C_{\text{HAC}} + C_{\text{Ac}^{-}} \quad (7)$$

In a solution without an externally induced electric field, the concentration of the charged species must also satisfy the electroneutrality constraint as shown by Equation (8).

$$\sum_i z_i C_i = 0 \quad (8)$$

In addition to the four equations discussed above (Equations (5)–(8)), the known solution pH and NaCl concentration can be used to fully resolve the system of equations in order to obtain the concentration of six chemical species ($\text{H}^{+}_{(\text{aq})}$, $\text{HAC}_{(\text{aq})}$, $\text{Ac}^{-}_{(\text{aq})}$, $\text{OH}^{-}_{(\text{aq})}$, $\text{Na}^{+}_{(\text{aq})}$, $\text{Cl}^{-}_{(\text{aq})}$). Considering that there are no ferrous ions present in the solution initially, the concentration of this species in the bulk solution was arbitrarily taken to be 10⁻⁶ M. The results obtained from the water chemistry calculation are shown in Fig. 1, where the ratio of undissociated acetic acid to the total acetic acid concentration is demonstrated for various pH values at 30 °C and 60 °C. At low pH values, the high concentration of hydrogen ion shifts the acetic acid dissociation equilibrium towards the left-hand side, so that most of the acetate species are in the form of undissociated acetic acid. On the other hand, the dissociation equilibrium dictates that the majority of acetate species is in acetate ion form at near neutral pH values. Fig. 1 also shows that a moderate change in temperature does not profoundly alter the solution speciation.

2.2.2. Electrochemical model

In order to quantify the polarization behavior of the studied system and also to ultimately estimate the corrosion rates, a comprehensive mathematical model of electrochemical/mass transfer behavior was developed similar to that discussed in detail elsewhere [20,21]. While the electrochemical reactions at the metal surface define the observed current/potential response of the system, the rate of these reactions themselves are dictated by the surface concentration of the involved electroactive species, which are determined by the mass transfer towards/away from the electrode surface. The mass transfer for a RDE consists of three parallel processes. Convective flow of the bulk fluid leading to a flux of the chemical species. Molecular diffusion as a result of the concentration gradient of the chemical species. Electromigration of the ionic species arising from the presence of an induced or spontaneous electric

Table 2
Summary of the experimental conditions.

Experimental Conditions	
Test apparatus	Rotating disk electrode Three-electrode glass cell
Temperature	30 °C
Rotation rate	2000 RPM
Electrode material	X65 mild steel
Supporting electrolyte	0.1 M NaCl
pH	3.0, 4.0, 5.0
Total acetate concentration	0 mM 1.66 mM (100 mass ppm) 8.30 mM (500 mass ppm) 16.60 mM (1000 mass ppm) 41.50 mM (2500 mass ppm)

Table 3
Equilibrium and reaction rate constants where $K = k_f/k_b$.

Parameter	Reference
$K_{HAc} = 10^{\left(-\frac{1500.65}{T} - 6.50923 \times \log(T) - 0.0076792 \times T + 18.67257\right)}$ (M)	[37]
$K_w = (10^{-3} \rho_w)^2 10^{-\left(a_1 + \frac{a_2}{T} + \frac{a_3}{T^2} + \frac{a_4}{T^3} + \left(a_5 + \frac{a_6}{T} + \frac{a_7}{T^2}\right) \log(10^{-3} \rho_w)\right)}$ (M ²) $a_1 = -4.098, a_2 = -3245.2, a_3 = 2.2362, a_4 = -3984E7,$ $a_5 = 13.957, a_6 = -1262.3, a_7 = 8.5641E5$	[38]
$k_{f,HAc} = 8.7 \times 10^5$ (1/s)	[39]
$k_{b,w} = 1.4 \times 10^{11}$ (1/M.s)	[40,41]

field. The flux of any given species i can be described through Equation (9) [23].

$$N_i = -z_i u_i F C_i \nabla \phi - D_i \nabla C_i + v_x C_i \quad (9)$$

The concentration distribution of each chemical species may be calculated by using the species conservation law, which can be mathematically expressed via Equation (10), also known as the Nernst-Planck equation.

$$\frac{\partial C_i}{\partial t} = -\nabla \cdot N_i + R_i \quad (10)$$

Considering the symmetrical geometry of the RDE, the tangential and radial species flux components of Equations (9) and (10) can be neglected. Furthermore, the mobility of ions can be estimated using Einstein-Smoluchowski relationship ($u_i = D_i/RT$), with diffusion coefficients listed in Table 4. Therefore, for a one-dimensional semi-infinite geometry in the direction x normal to the metal surface, Equations (9) and (10) can be simplified to Equations (11) and (12), respectively.

$$N_i = -D_i \frac{\partial C_i}{\partial x} - \frac{z_i D_i F C_i}{RT} \frac{\partial \phi}{\partial x} + v_x C_i \quad (11)$$

Table 4
Reference diffusion coefficients at 25 °C.

Species	Diffusion coefficient $\times 10^9$ (m ² /s)	Reference
HAc	1.29	[42]
Ac ⁻	1.089	[42]
H ⁺	9.312	[23]
OH ⁻	5.273	[42]
Na ⁺	1.334	[23]
Cl ⁻	2.032	[23,42]
Fe ²⁺	0.72	[23]

$$\frac{\partial C_i}{\partial t} = D_i \frac{\partial}{\partial x} \frac{\partial C_i}{\partial x} + \frac{\partial}{\partial x} \left(\frac{z_i D_i F C_i}{RT} \frac{\partial \phi}{\partial x} \right) - v_x \frac{\partial C_i}{\partial x} + R_i \quad (12)$$

The average bulk movement of the fluid in the direction normal to the surface is accounted for by the convective flow term $v_x C$, where v_x describes the velocity profile inside the diffusion layer. For a laminar flow regime of a RDE, the analytical solutions for the velocity profile (v_x) and the diffusion layer thickness (δ) are shown as Equation (13), where $a = 0.510$, and Equation (14), respectively [24].

$$v_x = -a\omega \left(\frac{\omega}{\nu} \right)^{1/2} x^2 \quad (13)$$

$$\delta = \left(\frac{3D_{lim}}{a\nu} \right)^{1/3} \left(\frac{\omega}{\nu} \right)^{-1/2} \quad (14)$$

Furthermore, the effect of homogeneous chemical reactions: acetic acid and water dissociation, are reflected by the R_i term in Equation (12). In a generic form, the rate of chemical reaction j (Reaction (15)) can be calculated as shown in Equation (16).

$$\sum_{r=1}^{n_r} C_r \rightleftharpoons \sum_{p=1}^{n_p} C_p \quad (15)$$

$$R_j = k_{f,j} \prod_{r=1}^{n_r} C_r - k_{b,j} \prod_{p=1}^{n_p} C_p \quad (16)$$

The rate of production (or consumption) of a species i (R_i in Equation (12)) can be expressed in a matrix format as Equation (17). The kinetic rate constants of the chemical reactions can be found in Table 3.

$$\begin{bmatrix} R_{H^+_{(aq)}} \\ R_{HAc_{(aq)}} \\ R_{Ac^-_{(aq)}} \\ R_{OH^-_{aq}} \end{bmatrix} = \begin{bmatrix} 1 & 1 \\ -1 & 0 \\ 1 & 0 \\ 0 & 1 \end{bmatrix} \times \begin{bmatrix} R_{HAc} \\ R_w \end{bmatrix} \quad (17)$$

Considering the discussion so far in this section, Equation (12) is applicable for each chemical species present in the system (H^+ , HAc, Ac⁻, OH⁻, Fe²⁺, Na⁺, Cl⁻) in order to determine their concentration distribution inside the diffusion layer. However, for this set of equations to be complete, the electric potential appearing in the electromigration term also needs to be specified. This parameter can be characterized through an additional relationship known as the “electroneutrality” constraint as described by Equation (8).

2.2.2.1. Initial and boundary conditions. At the initial time ($t = 0$), it can be assumed that a well-mixed solution comes into contact with the metal surface. Hence, the concentrations of the chemical species throughout the diffusion layer are constant known values, defined by the chemical equilibria of the solution, as discussed in Section 2.2.1.

At the bulk solution boundary, where $x = \delta$, the concentration of chemical species remains unchanged at all times ($t \geq 0$). Therefore, the boundary condition can be defined based on the known concentration of species, identical to those of the initial conditions.

The boundary condition at the metal/solution interface is based on the electrochemical reaction rate calculations. For an electroactive chemical species, the flux at the metal/solution boundary is equal to the rate of the corresponding electrochemical reaction. Therefore, for species i involved in electrochemical reaction j , the flux at the metal surface can be described through Equation (18).

Table 5
Electrochemical reaction rate relationships and parameters.

Charge transfer rates	n	α	m	E_{0j} vs. SHE (V)	$k_{0j, ref}$	E_a (kJ/mol)
$i_{c,H^+} = -n_{H^+} F k_{0,H^+} (C_{H^+}^s)^{m_{H^+}} e^{\left(\frac{-\alpha_{H^+} n_{H^+} F (E - E_{0,H^+})}{RT}\right)}$	1	0.43	0.5	0.00	7.58×10^{-8}	110.6
$i_{a,Fe} = n_{Fe} F k_{0,Fe} (C_{OH^-}^s)^{m_{OH^-}} e^{\left(\frac{(2-\alpha_{Fe}) F (E - E_{0,Fe})}{RT}\right)}$ $pH < 5$ or $C_{HAc} > 0$	2	0.50	1	-0.44	2.27×10^1	29.5
$i_{a,Fe} = n_{Fe} F k_{0,Fe} (C_{OH^-}^s)^{m_{OH^-}} e^{\left(\frac{2(1-\alpha_{Fe}) F (E - E_{0,Fe})}{RT}\right)}$ $pH = 5$ and $C_{HAc} = 0$	2	0.65	0	-0.44	2.05×10^{-5}	-

$$N_i|_{x=0} = -\frac{S_{ij} i_j}{n_j F} \quad (18)$$

Based on the analysis of the experimental results (Section 3.1), acetic acid was not considered to be involved in any electrochemical reaction. Also, considering that the water reduction reaction is not significant at the corrosion potential, it was not included in the model. Hence, the electrochemical reactions considered in the model consisted only of one cathodic reaction, hydrogen ion reduction (Reaction (3)), and one anodic reaction, iron oxidation (Reaction (2)). Due to negligible concentration of H_2 in the solution (which is stripped out by the nitrogen bubbling through the solution), no significant contribution of hydrogen oxidation reaction over the potential range of interest is expected. Hence, the current density resulting from hydrogen ion reduction was calculated in the form shown in Table 5, which considers the cathodic half reaction only. The related kinetic parameters, including the transfer coefficient α , the reaction rate constant k_0 , and the reaction order m_{H^+} , were obtained based on the experimental data as discussed in Section 4.

The current density resulting from iron dissolution (Reaction (2)) can be calculated by considering the anodic half reaction only, since the ferrous ion reduction may also be assumed negligible, because of its low concentration and the potential range of interest. The rate of iron oxidation reaction, at the active dissolution range observed in lower pH values (e.g. below 5), is known to have a first order pH dependence [25,26,30]. It is also known that the mechanism of iron oxidation reaction at the vicinity of corrosion potential changes at near neutral pH values [25,26,28]. Therefore, two different reaction rate relationships were considered, one for lower and the other for higher pH values, as shown in Table 5. These relationships are based on previously reported behavior, with a strong pH dependence in more acidic solutions and no dependence at higher pH values [25,28]. The change of mechanism is also reported to coincide with a change of apparent Tafel slope. The kinetic parameters reported in Table 5 were obtained based on the experimental results of the present study, as further discussed in Section 4.

The current/potential relationships used to calculate the rate of electrochemical reactions are listed in Table 5. The negative sign in Equation (18) is due to a sign convention where cathodic currents are taken as negative while anodic currents are positive. Furthermore, all the reactions are written in “cathodic” form (e.g. Reactions (2) and (3)), so the reactants on the left hand side are represented with a negative stoichiometric coefficient (S_{ij}) and the products on the right hand side are represented as positive values.

Equation (18) can be expanded using a matrix notation in order to include all the electro-active species:

$$\begin{bmatrix} N_{Fe^{2+}(aq)}|_{x=0} \\ N_{H^+(aq)}|_{x=0} \end{bmatrix} = \begin{bmatrix} 1 & 0 \\ 0 & -1 \end{bmatrix} \times \begin{bmatrix} i_{Fe} \\ i_{H^+} \\ F \end{bmatrix} \quad (19)$$

For non-electroactive species, the flux at the metal surface is zero, as it is a non-porous non-reactive barrier:

$$N_i|_{x=0} = 0 \quad (20)$$

The flux Equations (19) and (20) can be used to describe the boundary conditions for all chemical species at the metal surface.

In order to calculate the cathodic and anodic current in Equations (19), the potential at the metal surface (E) needs to be known. That is true for the case where electrode potential is the controlled parameter (such as in potentiodynamic measurements). However, when the calculations are done to obtain the corrosion rates, the potential at the metal surface is not explicitly known. In that case, an additional relationship is required to relate the potential at the metal surface to other known parameters. This can be achieved by introducing the charge conservation at the electrode surface based on the mixed potential theory. That suggests the net current resulting from all j electrochemical reactions is equal to zero, mathematically expressed as Equation (21).

$$\sum_j i_j = 0 \quad (21)$$

2.2.2.2. Numerical solution. Table 6 summarizes all the relevant mathematical equations required to develop a comprehensive mathematical model as discussed above. These equations form a set of non-linear, coupled, partial differential equations to be solved numerically. Considering a simple one-dimensional computational space, the finite difference method can be used to solve the equations. This method is commonplace in mathematical modeling of electrochemical systems with similar geometry and has been discussed in detail elsewhere [23,29].

The partial differential equations are discretized using second order Taylor's series approximations. The time integration is done explicitly, using Euler approximation. The resulting algebraic equations can be written in a matrix format, as a tri-diagonal coefficient matrix multiplied by the unknown concentrations and solution potential. The final solution can then be obtained through different solution algorithms such as Neman's “BAND” open-source code where it is solved by LU decomposition method [23,29]. The presence of nonlinear terms, such as those in the electromigration or chemical reactions relationships, makes some of the terms in the coefficient matrix to be a function of other concentrations and/or potential, i.e. they are not explicitly known. In the approach used in

Table 6
Summary of equations used in the mathematical model.

Electrode surface boundary	
$N_{i _{x=0}} = -\frac{S_{ij}}{n_i F}$	for electroactive species
$N_{i _{x=0}} = 0$	for non-electroactive species
$\sum_i z_i C_i = 0$	
$\sum_j i_j = 0$	for unknown electrode potential
Diffusion layer	
$\frac{\partial C_i}{\partial t} = D_i \frac{\partial^2 C_i}{\partial x^2} + \frac{\partial}{\partial x} \left(\frac{z_i D_i F C_i}{RT} \frac{\partial \phi}{\partial x} \right) - \nu_x \frac{\partial C_i}{\partial x} + R_i$	for all species
$\sum_i z_i C_i = 0$	
Bulk boundary conditions	
$C_i = C_i^b$	for all species
$\Phi = 0$	arbitrary reference potential

the present model, the final solution was obtained iteratively by using an initial guess for the unknown terms of the coefficient matrix –usually the last calculated value of the unknown term– until the desired accuracy ($R^2=10^{-12}$) was achieved.

3. Results and discussion

In general, the reduction of any weak acid in an aqueous solution, including acetic acid used in the present study, is thermodynamically identical to that of hydrogen ion reduction. This can be readily shown through the reversible potential of the two reactions based on the Nernst equation, where the concentration of the weak acid and its conjugate base are defined by the chemical equilibrium of the weak acid dissociation. Therefore, the difference between the hydrogen ion reduction and the direct reduction of the weak acid resides only in the kinetics of these electrochemical reactions. The two reactions can therefore be distinguished by investigating the cathodic polarization behavior of the system in the charge transfer controlled current range.

The experimental conditions in the present study were designed so that the electrochemical activity of acetic acid, as an additional oxidizing species, could be properly distinguished. In these experiments, at a fixed solution pH the concentration of acetic acid was varied. Since the charge transfer rate from hydrogen ion reduction is constant at a constant pH, any increase in the charge transfer controlled current density indicates that the direct reduction of acetic acid is significant and it is occurring in parallel. In contrast, if the charge transfer controlled current density remain unchanged for different acetic acid concentrations, one can conclude that the direct reduction of acetic acid is not significant.

Furthermore, all the reported polarization curves in this section show a significant increase in mass transfer limiting current, as the concentration of acetic acid is increased. However, the behavior of the mass transfer limiting current is the same irrespective of whether acetic acid is directly reduced or not, thus, the variation in the limiting current density cannot be used to determine the electrochemical activity of acetic acid. The effect of acetic acid concentration on charge transfer controlled currents is presented in section 3.1 below, and its effect on limiting currents is discussed in section 3.2.

3.1. Electrochemical activity of acetic acid

The typical polarization curves at pH 3, pH 4 and pH 5 for increasing acetic acid concentrations are reported in Figs. 2–4. In these graphs the anodic polarization curves typically consist of a linear range, just above the OCP, followed by a current maximum and another linear range at more positive potentials. The cathodic

polarization curves also consist of a linear range just below the OCP, associated with the hydrogen ion reduction, followed by the mass transfer limiting current and another linear range at more negative potentials associated with the water reduction reaction. The discussion below is mostly focused on the electrochemical reactions in the vicinity of the OCP. That is, the anodic current densities below the anodic current maximum and cathodic current densities up to the limiting current.

Fig. 2 shows the polarization curves obtained at pH 5, where a significant change was observed by addition of 0.60 mM undissociated acetic acid ($C_{t,HAc} = 1.66$ mM). The shift of OCP towards more positive potentials can be explained when considering that the cathodic polarization curve was under mass transfer control in the absence of acetic acid, and the significant increase of the limiting current by addition of acetic acid leads to an increased OCP. In the presence of acetic acid, a Tafel behavior is clearly observed in the cathodic polarization curves, particularly when the acetic acid concentration was further increased. The comparison of the charge transfer controlled currents did not indicate any increase in charge transfer rates that could be associated with direct reduction of acetic acid. Actually, one can observe a slight decrease with increasing acetic acid concentration, a behavior that will be discussed further below. The cathodic polarization curves obtained at acetic acid concentrations up to 15.1 mM ($C_{t,HAc} = 41.5$ mM) further support these observation.

The anodic polarization curves in Fig. 2 show a significant change in the polarization behavior by addition of 0.60 mM undissociated acetic acid. In the presence of acetic acid, a Tafel slope of approximately 40 mV was observed, which agrees well with the typical Tafel slopes reported in the literature for anodic iron dissolution in acidic solutions [13,25]. The same 40 mV Tafel slope was obtained in the experimental data reported below for lower pH values with or without acetic acid present. However at pH 5, as shown in Fig. 2, a notably different behavior with an apparent ~90 mV Tafel slope and a significantly higher rates of the anodic dissolution reaction was observed when no acetic acid was present. A similar effect has been repeatedly reported in the literature that suggests a significant change in the electrochemical behavior of the iron dissolution reaction occurs as the solution pH is increased towards neutral values (pH 5 and higher) [25,26,30,31]. This can be better understood by considering the well-known categorization of El Miligy et al. [26] who suggested

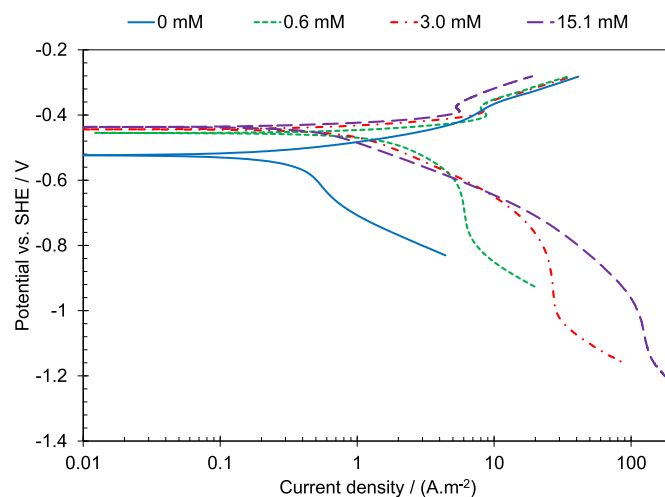


Fig. 2. Polarization behavior of X65 mild steel in solution of pH 5, at 30 °C, 2000 rpm, 0.1 M NaCl, and undissociated acetic acid concentrations 0 mM, 0.6 mM ($C_{t,HAc} = 1.7$ mM), 3.0 mM ($C_{t,HAc} = 8.3$ mM), and 15.1 mM ($C_{t,HAc} = 41.5$ mM).

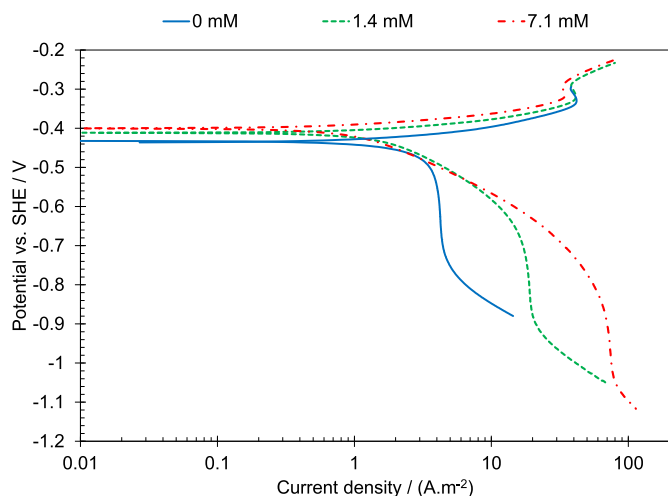


Fig. 3. Polarization behavior of X65 mild steel in acidic solution of pH 4, at 30 °C, RDE, 2000 rpm, 0.1 M NaCl, and undissociated acetic acid concentrations 0 mM, 1.4 mM ($C_{t,HAC} = 1.7$ mM) and 7.1 mM ($C_{t,HAC} = 8.3$ mM).

that the iron dissolution in mildly acidic environments passes through four ranges as the potential is increased towards more positive values. The four ranges are characterized with different Tafel slopes and reaction orders, depending on the solution pH and the electrode potential [26]. Ordered from more negative towards more positive potentials, the authors categorized these ranges as *active dissolution*, characterized by 30–40 mV Tafel slope, *transition*, characterized by observation of the first current maximum, *pre-passivation*, characterized by a 120 mV Tafel slope, and *passivation* that occurs after the second current maximum [26]. The 40 mV Tafel slope observed in most conditions in the present study is a characteristic behavior of the iron oxidation in the *active dissolution* range. The increased Tafel slope at higher pH values suggests that the iron dissolution was at the *transition/pre-passivation* range. Nevertheless, the above discussion does not explain why the presence of acetic acid shifts the OCP back into the active dissolution range. The complete picture can only be seen when considering the behavior of cathodic currents as well. The comparison of the cathodic polarization curves in Fig. 2, shows that at pH 5 when no acetic acid was present, the mass transfer limited cathodic currents were extended into the potential range well above the OCP, up to -0.425 V (vs. SHE). That means, the pH at the surface remains significantly higher than the pH in the bulk solution even when the electrode was polarized anodically. Therefore, the change in the electrochemical behavior of the iron dissolution reaction with addition of acetic acid is merely a result of increased cathodic limiting currents and consequently decreased surface pH to that of the bulk solution at potentials equal or higher than OCP (anodic potential range).

A smaller, but notable decrease of the anodic dissolution rate was observed as the acetic acid concentration was further increased. The anodic current densities at these conditions were slightly retarded while the observed Tafel slopes remained unchanged, what was observed as a slight shift of open circuit potentials toward more positive values. This same behavior has been frequently reported in the literature, suggesting that acetic acid slightly inhibits the iron dissolution reaction [10,12,17].

The polarization curves at pH 4 with and without acetic acid are shown in Fig. 3. The Tafel behavior is clearly observed in the solutions containing acetic acid, with charge transfer controlled currents showing no significant increase with increasing acetic acid concentration. The inhibiting effect on the anodic dissolution

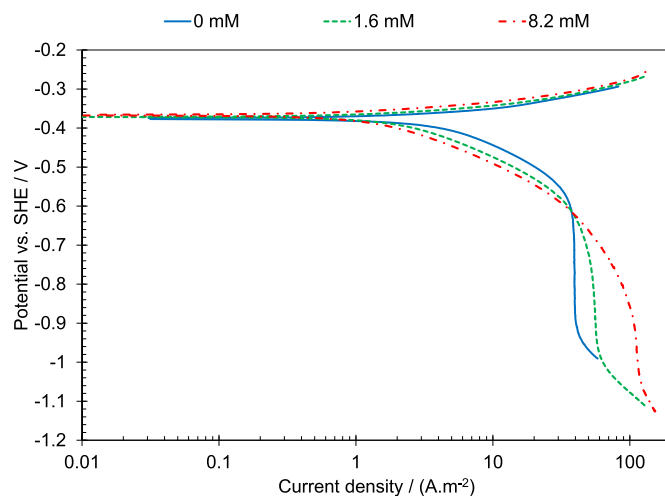


Fig. 4. Polarization behavior of X65 mild steel in acidic solution of pH 3, at 30 °C, RDE, 2000 rpm, 0.1 M NaCl, and undissociated acetic acid concentrations 0 mM, 1.6 mM ($C_{t,HAC} = 1.7$ mM), and 8.2 mM ($C_{t,HAC} = 8.3$ mM).

reaction can be clearly observed with the increase in acetic acid concentration.

The polarization curves at pH 3 are shown in Fig. 4. This condition is of particular significance, since the Tafel behavior is clearly observed even when no acetic acid was present. At this condition also, increasing the acetic acid concentration did not result in any increase of the charge transfer controlled cathodic current (in the Tafel range), further supporting the argument that acetic acid is not directly reduced at the steel surface. Actually, an opposite effect was clearly observed that suggests a significant inhibiting effect of acetic acid on cathodic currents. The similar effect was noticeable at pH 5 and pH 4 as well (in Figs. 2 and 3), however, it was not as clearly discernible. The inhibitive effect on the anodic dissolution was also observed at pH 3 similar to what was shown at higher pH values.

Based on the polarization behavior of the studied system, it is reasonable to conclude that acetic acid is not a significant electroactive species in the conditions considered in the present study (i.e. if there is any cathodic current resulting from reduction of acetic acid it is overshadowed by its inhibiting effect on the charge transfer rate of hydrogen ion reduction). Specifically, the results shown at pH 5 and 15.08 mM acetic acid, where $C_{HAC}/C_H^+ \approx 1500$, suggest that the reaction rate constant for acetic acid direct reduction is at least three orders of magnitude lower than that of hydrogen ion reduction, considering that the over potential is identical for both reactions [1] (based on the Nernst equation with concentration terms defined by acetic acid equilibrium). Therefore, it can be assumed that the contribution of direct acetic acid reduction in the typical conditions encountered in the oil and gas industry would be insignificant as compared to hydrogen ion reduction. Thereby, the corrosion process of mild steel in mildly acidic solutions containing acetic acid is a result of only two electrochemical reactions: hydrogen ion reduction as the sole cathodic reaction and the iron dissolution as the sole anodic reaction. However, the polarization curves reported in Figs. 2–4 suggest that the presence of acetic acid significantly affects the corrosion process, first by increasing the mass transfer limiting current and second, by inhibiting the charge transfer rate of both the cathodic hydrogen ion reduction reaction and the anodic iron dissolution reaction. These processes are the subjects of further discussions in the following sections.

3.2. Effect of acetic acid on limiting current

The reported polarization curves in Figs. 2–4 showed that the limiting current density is significantly affected by acetic acid concentration. As concluded in the previous section, the hydrogen ion reduction is the only cathodic reaction in the present discussion. The limiting current is therefore a result of the depletion of hydrogen ion concentration at the metal surface. In accordance to this local change of pH at the limiting current condition, the local chemical equilibrium of acetic acid (Reaction (1)) at the surface shifts towards acetic acid dissociation. Consequently, the acetic acid dissociation is acting as an additional source of hydrogen ions, further increasing the limiting current. Therefore, the cathodic limiting current is consist of two components:

- The mass transfer of hydrogen atoms from the bulk to the metal surface followed by their reduction at the surface.
- The mass transfer of undissociated acetic acid followed by homogeneous dissociation to hydrogen ions and acetate ions inside the diffusion layer, succeeded by reduction of the produced hydrogen ion at the surface.

The effect of acetic acid on mass transfer rates was also studied in experiments at a fixed solution composition while the rotation speed of the RDE was varied. Fig. 5 shows the typical polarization curves obtained at 125, 500, and 2000, rpm at pH 3 where no acetic acid was present (Fig. 5A) and when the solution contained 8.13 mM undissociated acetic acid (Fig. 5B).

For the case where the hydrogen ion reduction reaction follows the acetic acid dissociation reaction, the limiting current density can be expressed through Equation (22), for a RDE flow geometry [32].

$$i_{lim} = \frac{nFD (C_{H^+}^b + C_{HAc}^b)}{1.61 D^{\frac{1}{2}} \omega^{-\frac{1}{2}} \nu^{\frac{1}{6}} + \left(\left(\frac{D}{(k_{f,HAc} + k_{b,HAc})} \right)^{\frac{1}{2}} / K_{HAc} \right)} \quad (22)$$

In the absence of acetic acid, the second term in the denominator of Equation (22) as well as the acetic acid concentration term disappear. Hence, Equation (22) reduces to the well-known Levich equation where the limiting current is proportional to $\omega^{0.5}$. The results obtained in the absence of acetic acid at pH 3 were found to agree well with this expected trend, as shown in Fig. 6.

In the presence of acetic acid, Equation (22) suggests that the behavior of limiting current vs. $\omega^{0.5}$ would depend on the kinetics and the equilibrium constant of the acetic acid dissociation reaction as well. Nevertheless, the linear behavior obtained in the presence of acetic acid, as shown in Fig. 6, suggests that the flow dependent term (first term in denominator) has remained significantly larger than the chemical reaction dependent term, even at rotation speeds as high as 2000 rpm. Considering that the denominator of Equation (22) is defined only by the environmental conditions and physiochemical parameters, the limiting currents in the system studied here could therefore be represented by the superposition of hydrogen ion and acetic acid mass transfer from the bulk. That is shown to be indeed the case in Fig. 7, where the limiting current is presented as a function of the sum of hydrogen ion and undissociated acetic acid concentrations. It should be noted that the different diffusion coefficient of acetic acid and hydrogen ion, as the only species dependent parameter, should be accounted for in this treatment. The linear behavior of the trendline and the fact that it is crossing the origin, justifies this approach. These results suggest that acetic acid is a strong buffer in the sense that the kinetics and the equilibrium of its dissociation equilibrium allows this species to

readily dissociate and buffer the hydrogen ion concentration at the metal surface, whenever the hydrogen ion concentration deviates from the equilibrium. In other words, undissociated acetic acid is primarily a “carrier” for hydrogen ions and increases the effective concentration of hydrogen ions in mild steel corrosion.

4. Estimation of physiochemical parameters

The mathematical model developed in Section 2.2.2, was used to obtain the physicochemical parameters of the studied system. This was achieved by determining appropriate values by fitting the model to the experimental data. The kinetic parameters of the electrochemical (hydrogen evolution and iron dissolution) reactions were obtained by using only the experimental data where no acetic acid was present. This step was considered necessary to assure that the estimated parameters were free of any interference due to the presence of acetic acid. Fig. 8 shows the comparison of the model (dotted black lines) with the experimental data at pH 3 to pH 5, using the estimated parameters shown in Table 5.

The transfer coefficient for the hydrogen ion reduction (0.43) was slightly lower than the commonly accepted theoretical value of 0.5, however, similar deviations have been previously reported [33,34]. The iron dissolution reaction showed a significant change in the kinetic parameters at pH 5 (compared to pH 3 and pH 4) where the Tafel slope increased from 40 mV at pH 4 to approximately 90 mV at pH 5. As discussed above, this behavior has been frequently reported in the previous studies [25,26,30,31], and suggests that at this environmental condition the mechanism of iron dissolution in the vicinity of corrosion potential is no longer in the active dissolution range. Based on this observation, a different charge transfer relationship was used for this particular condition (Table 5). As noted in section 3.1, this behavior was only observed at pH 5 when no acetic acid was present.

4.1. Inhibiting effect of acetic acid

Considering that the direct acetic acid reduction was shown to be insignificant in the conditions of the present study, the model developed above based solely on hydrogen ion reduction and iron dissolution reactions, should be able to describe the steady state voltammograms obtained in the presence of acetic acid. However, the inhibiting effect of undissociated acetic acid on the charge transfer rates also needs to be quantified for more accurate prediction of both the polarization curves and corrosion rates.

The inhibiting effect of acetic acid on the anodic and cathodic charge transfer rates was quantified in terms of its adsorption on the metal surface acting as a weak corrosion inhibitor that results in blockage of the active sites of the electron transfer reactions. However, considering numerous surface active species, such as water, chloride ions, as well as anodic and cathodic reaction intermediate species and the non-uniformity of the steel surface, a detailed mechanistic description of this phenomena is well beyond the scope of the present study, hence, a semi-empirical approach was employed. In this approach, the rate of electrochemical reactions in the presence of acetic acid was assumed to follow Equations (23) and (24):

$$i_{H^+,HAc} = i_{H^+} (1 - \theta_c) \quad (23)$$

$$i_{Fe,HAc} = i_{Fe} (1 - \theta_a) \quad (24)$$

Since the reaction rate constants were known from the condition without acetic acid present, the surface coverage of acetic acid (θ) could be determined by the apparent rate constants from the experimental data as shown in Equation (25). Here $k_{0,HAc}$ is the

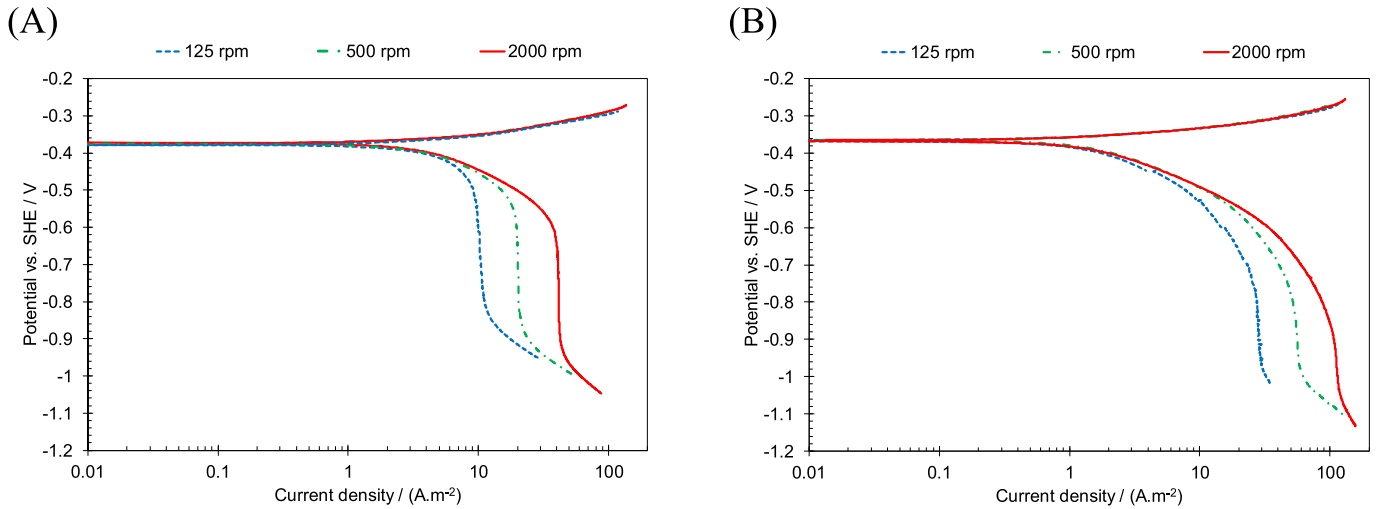


Fig. 5. Polarization behavior of X65 mild steel in acidic solution of pH 3, at 30 °C, 0.1 M NaCl, and various rotation speeds. A) $C_{HAc}=0$ mM, B) $C_{HAc}=8.2$ mM.

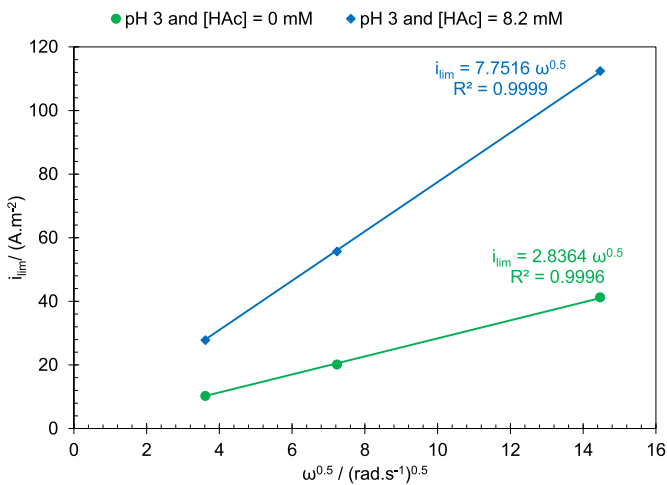


Fig. 6. The behavior of the limiting current density vs. square root of rotation speed in acidic solution of pH 3, at 30 °C, 0.1 M NaCl.

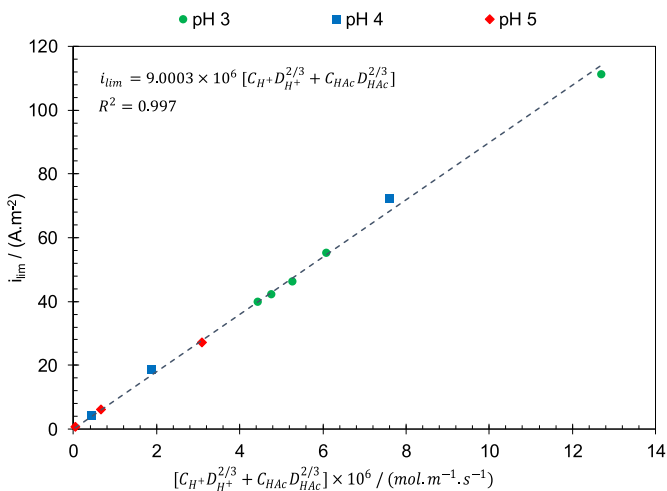


Fig. 7. Limiting current density at various hydrogen ion and undissociated acetic acid concentrations on X65 RDE, 2000 rpm, 30 °C, 0.1 M NaCl and C_{HAc} from 0 mM to 8.2 mM.

apparent reaction rate constant in the presence of acetic acid and k_0 is the reaction rate constant at similar conditions but when acetic acid was not present.

$$\frac{k_{0,HAc}}{k_0} = (1 - \theta) \quad (25)$$

As noted in Equation (25), the calculation of θ required the k_0 where no acetic acid was present to be known explicitly. As shown in Figs. 2–4, pH 3 was the only condition where the pure charge transfer controlled cathodic current was observed without acetic acid being present, and the anodic polarization curves were not affected by local pH due to cathodic mass transfer limitation. Hence, the k_0 values could be obtained from the experimental data, directly. Thereby, pH 3 was selected as the base condition for the discussion on the inhibitive effect of acetic acid on the charge transfer rates. Fig. 9 demonstrates the values of surface coverage obtained as described via Equation (25), using the experimental data at pH 3 and extended acetic acid concentrations.

The coverage effect associated with the acetic acid adsorption shows a logarithmic trend with the undissociated acetic acid

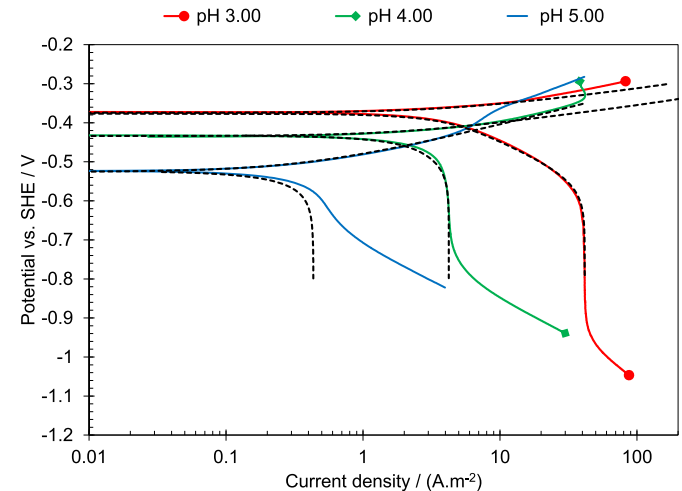


Fig. 8. Comparison of the experimental and calculated (dotted back lines) polarization behavior of X65 mild steel in acidic solutions in the absence of HAc, at 30 °C, 0.1 M NaCl, RDE, 2000 rpm, and various pH values.

concentration, as shown in Fig. 9. Transforming this functionality (Equation (26) to Equation (27)) shows that acetic acid follows a Temkin type adsorption isotherm.

$$\theta = A \ln(C_{HAc}) + B \quad (26)$$

$$e^{(r\theta)} = KC_{HAc} \quad (27)$$

where $K = e^{B/A}$ and $r = 1/A$. However, the observed inhibiting effect was different for the cathodic and anodic reactions. That is due to the semi-empirical treatment of these parameters where the effect of the numerous surface active species and non-uniform steel surface are all lumped into the two constants of Equation (26). The difference in the observed inhibitive effect on the cathodic and anodic currents suggests a competitive adsorption scenario. At anodic currents, acetic acid is competing with electrochemical hydroxide adsorption as the reactions intermediate of the iron dissolution [25,35,36], while at cathodic currents it is the electrochemical hydrogen ion adsorption in competition with acetic acid.

Fig. 10 is a comparison of the experimental results at pH 3 with those calculated by the model. The agreement of the results showed that the inhibitive effect of acetic acid was properly reflected through the Temkin type adsorption isotherms discussed above.

4.2. Temperature effect

An increase in temperature affects the charge transfer and the mass transfer rates as well as the adsorption of acetic acid, and the solution speciation (as discussed in section 2.2.1). Fig. 11 shows the experimental polarization curves obtained at pH 3 for 30 °C, 40 °C and 50 °C, A) in the absence and B) in the presence of acetic acid.

The effect of temperature on mass transfer rate is through temperature dependence of the terms in the Nernst-Planck equation, which includes the diffusion coefficient in molecular diffusion and electromigration terms. The flow velocity (v_x) in convective flow term is affected by the temperature dependence of physical properties of water, such as viscosity and density. The temperature dependence of these parameters are summarized in Table 7.

The effect of temperature on charge transfer rate can be

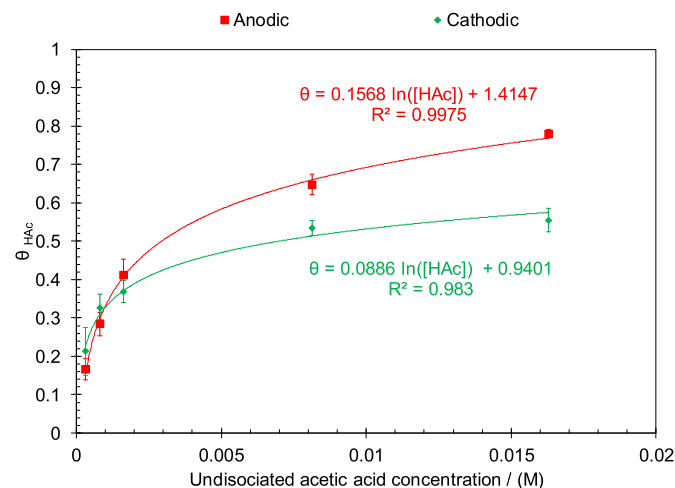


Fig. 9. The variation of θ , defined by Equation (25), as a function of undissociated acetic acid concentration for cathodic currents (green diamonds) and anodic currents (red squares). Error bars are based on the standard deviation of at least three repeats. (For interpretation of the references to colour in this figure legend, the reader is referred to the web version of this article.)

characterized by an Arrhenius law type of expression and the activation energy of the electrochemical reactions. Fig. 12 shows the temperature dependence of the apparent reaction rate constants, where the slope of the trendline represents the activation energy of a given reaction (E_a/R). Therefore, the temperature dependence of the electrochemical reactions can be expressed through van't Hoff's law:

$$k_{0j} = k_{0j,ref} e^{\left(-\frac{E_a}{R} \left(\frac{1}{T} - \frac{1}{303}\right)\right)} \quad (28)$$

The effect of temperature on inhibition by acetic acid can be discussed in terms of the parameter θ as shown in Equation (27), where K is the adsorption equilibrium constant with an Arrhenius type temperature dependence ($K = K_0 e^{-E_a/RT}$) and $r = b/RT$. Therefore, Equation (26) can be restated as Equation (29) to accommodate for the temperature effect.

$$\theta = \frac{RT}{b} (\ln([HAc]) + \ln(K_0)) - \frac{E_a}{b} \quad (29)$$

The only unknown parameter in Equation (29) is E_a , the activation energy of the acetic acid adsorption equilibrium constant. As shown in Equation (29), E_a is represented by the intercept of the trendline ($-E_a/b$) in a θ vs. T graph as shown in Fig. 13. From these results, the temperature effect on the inhibition by acetic acid is expressed by the last two equations shown in Table 7.

The temperature dependence of the physiochemical parameters, as summarized in Table 7, were incorporated into the model and the predicted voltammograms were compared with experimental data. Fig. 11A shows the comparison for the case without any acetic acid present, while the predicted voltammograms for a solution at pH 3 and 8.2 mM undissociated acetic acid concentration is shown in Fig. 11B. Here again a reasonable agreement was found while at more negative potentials close to limiting current densities, slight deviations between the predicted apparent Tafel slopes and the measurements were observed.

The effect of increased temperature in the presence of acetic acid is demonstrated in Fig. 14 based on the prediction of the model at pH 5. These results shows a synergistic effect of temperature with undissociated acetic acid concentration on the corrosion rates that further elucidates the inconsistent behavior of corrosion rates in the presence of acetic acid as reported in the literature (see

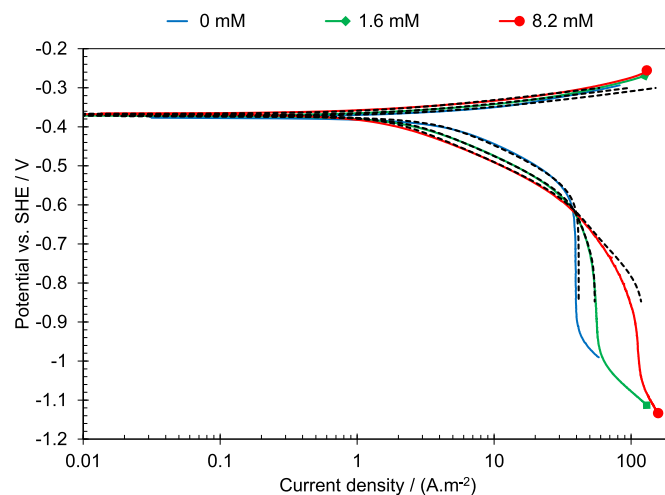


Fig. 10. Comparison of the experimental and calculated (dotted black lines) polarization behavior of X65 mild steel in acidic solutions demonstrating the inhibitive effect of acetic acid of pH 3, at 30 °C, 0.1 M NaCl, RDE, 2000 rpm.

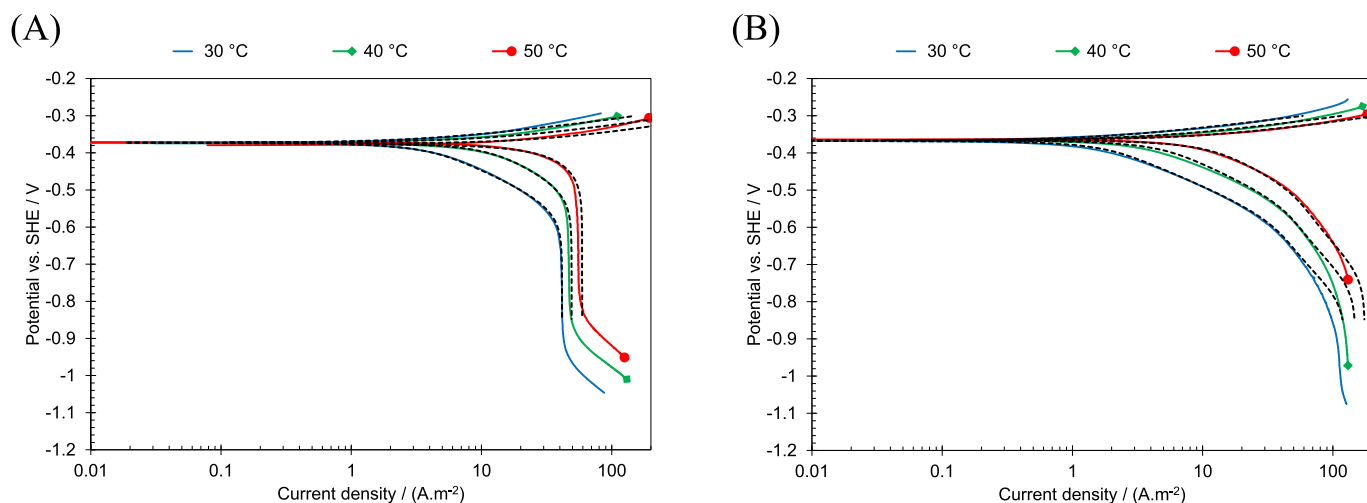


Fig. 11. Comparison of the experimental and calculated (dotted black lines) polarization behavior of X65 mild steel in acidic solutions demonstrating the temperature effect at pH 3, 0.1 M NaCl, 2000 rpm RDE at 30 °C (blue line), 40 °C (green line), and 50 °C (red line). A) 0 ppm HAC, B) 500 ppm HAC. (For interpretation of the references to colour in this figure legend, the reader is referred to the web version of this article.)

Table 7
Temperature dependence of the physiochemical properties.

Parameter	Relationship	Reference
Water density (kg/m ³)	$\rho_w = 753.596 + 1.87748 T - 0.003562 T^2$	[28]
Water viscosity (cP)	$\mu = \mu_{ref} 10^{\left(\frac{1.1709 (T_{ref}-T) - 0.001827 (T_{ref}-T)^2}{(T-273.15)+89.93} \right)}$ $T_{ref} = 293.15 K, \mu_{ref} = 1.002 cP$	[43]
Diffusion coefficient	$D_i = D_{i,ref} \frac{T}{T_{ref}} \frac{\mu_{ref}}{\mu}$	[23]
HAc adsorption, cathodic	$\theta_c = 8.86 \times 10^2 \frac{T}{303.15} \left(\ln(C_{HAc}) + 10.61 + \frac{-61385}{R} \left(\frac{1}{T} - \frac{1}{303.15} \right) \right)$	This study
HAc adsorption, anodic	$\theta_a = 1.57 \times 10^{-1} \frac{T}{303.15} \left(\ln(C_{HAc}) + 9.02 + \frac{-2248}{R} \left(\frac{1}{T} - \frac{1}{303.15} \right) \right)$	This study

Section 1). Fig. 14 shows that a maximum corrosion rate exists at each condition, which is increased at higher temperatures and is greatly influenced by acetic acid concentration. The decreasing trend of corrosion rates, observed in Fig. 14 is a result of acetic acid

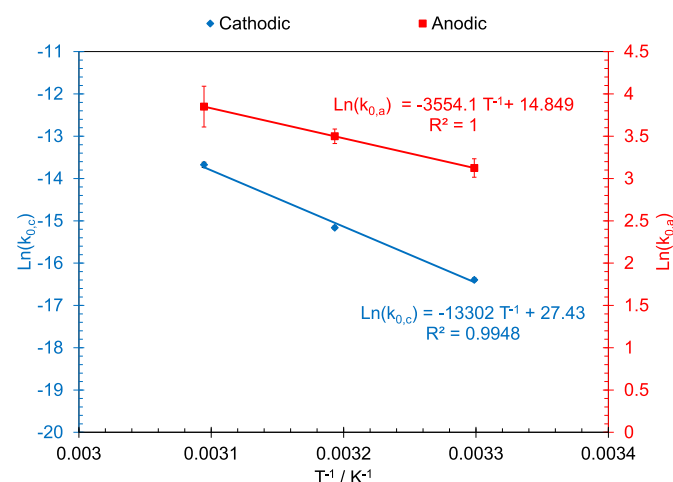


Fig. 12. Temperature dependence for the reaction rate constant without acetic acid present at pH 3, 0.1 M NaCl, for hydrogen ion reduction (blue diamonds) and iron oxidation (red squares). Error bars are based on the standard deviation of at least three repeats. (For interpretation of the references to colour in this figure legend, the reader is referred to the web version of this article.)

inhibitive effect on the charge transfer cathodic and anodic currents when the corrosion current is controlled by the rate of electrochemical reactions. Whereas, the increasing effect on the corrosion rate stems from the buffering ability of acetic acid and the resulting increase in limiting currents, when the corrosion current is under mass transfer control. At elevated temperatures, the increased rate of anodic and cathodic reactions shifts the corrosion current towards the mass transfer limiting range, as readily observed in the polarization behavior in Fig. 11. This combined effect leads to extremely high corrosion rates at elevated temperatures in the presence of acetic acid.

5. Corrosion rate prediction

The performance of the mathematical model developed in the previous sections was further examined with the comparison of the estimated corrosion rates with the experimental data. Fig. 15 is the comparison of the corrosion rate data obtained by linear polarization measurements at pH 3, pH 4, and pH 5 with and without acetic acid present. At pH 3 and pH 4 where the corrosion current is mostly under charge transfer control, increasing acetic acid concentration decreased the corrosion rates. At pH 5 and in the absence of acetic acid, the corrosion current was under mass transfer control (Fig. 2), therefore, by addition of 0.6 mM undissociated acetic acid, the corrosion rate was rapidly increased, but further increase of acetic acid resulted in a slightly lower corrosion rate. The effect of acetic acid on the observed corrosion rates shown in Fig. 15 was in

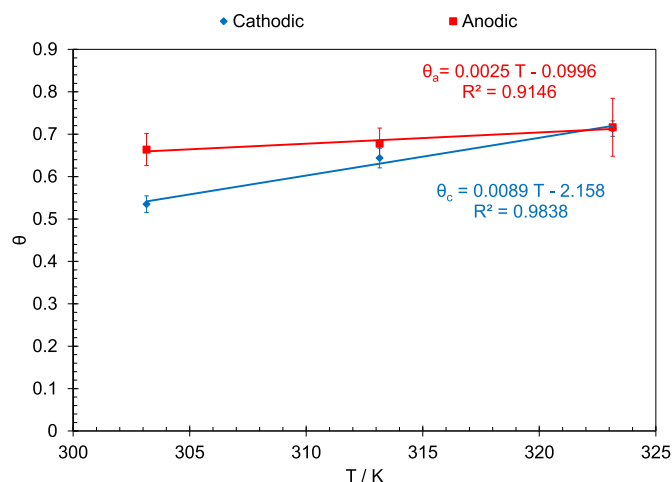


Fig. 13. Temperature dependence for acetic acid adsorption at pH 3, 0.1 M NaCl, and $C_{\text{HAc}} = 8.2$ mM, for hydrogen ion reduction (blue diamonds) and iron oxidation (red squares). Error bars are based on the standard deviation of at least three repeats. (For interpretation of the references to colour in this figure legend, the reader is referred to the web version of this article.)

complete agreement with the expected behavior as discussed in Section 3.

The performance of the model was further examined in the parity plot shown in Fig. 16 where the experimental data was compared with the calculated corrosion rates for a wider range of environmental conditions and solution compositions ($22\text{ }^{\circ}\text{C} < T < 60\text{ }^{\circ}\text{C}$, $2 < \text{pH} < 5$, $0\text{ mM} < C_{\text{t,HAc}} < 16.6\text{ mM}$, $125\text{ rpm} < \text{rotation speed} < 2000\text{ rpm}$). Most of the calculated data points are within 20% of the measured values and in almost every case within a factor of two.

6. Conclusions

- The experimental results and the quantitative analysis reported in the present study showed that the direct acetic acid reduction does not significantly contribute to the cathodic currents in acidic solutions.
- Acetic acid was shown to be a strong buffer which was fully dissociated under mass transfer limiting conditions, meaning

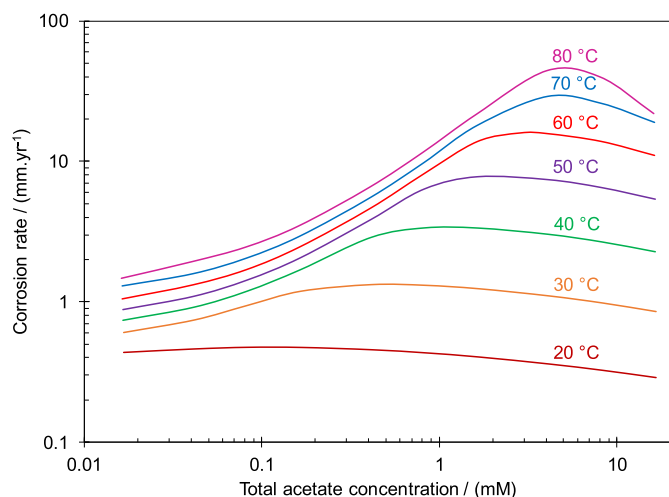


Fig. 14. The estimated corrosion rates for mild steel in pH 5, 0.1 M NaCl, 2000 rpm RDE with respect to temperature and total acetic acid concentration.

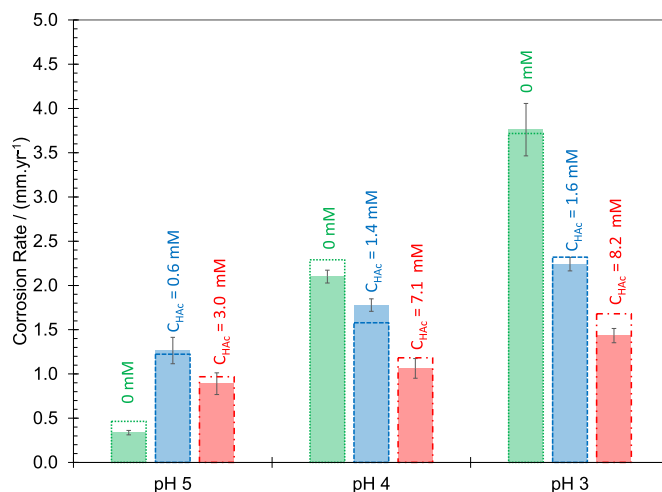


Fig. 15. Comparison of the experimental and calculated corrosion rates of X65 mild steel in acidic solutions, at $30\text{ }^{\circ}\text{C}$, 0.1 M NaCl, 2000 rpm, at various pH and $C_{\text{t,HAc}}$ values. Dashed boxes show the predicted values. Error bars are based on the standard deviation of at least three repeats. (For interpretation of the references to colour in this figure legend, the reader is referred to the web version of this article.)

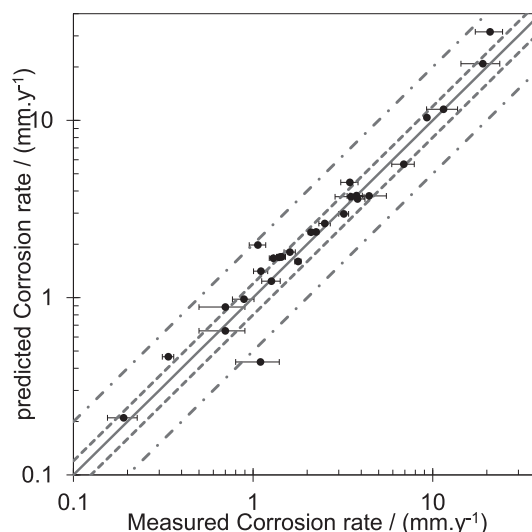


Fig. 16. Comparison of the predicted corrosion rates with experimental results for a wide range of parameters. $22\text{ }^{\circ}\text{C} < T < 60\text{ }^{\circ}\text{C}$, $2 < \text{pH} < 5$, $0\text{ mM} < C_{\text{t,HAc}} < 16.6\text{ mM}$, $125\text{ rpm} < \text{rotation speed} < 2000\text{ rpm}$. Additional experimental data from Zheng et al. [44] and George et al. [13]. Dashed lines and the dotted dashed lines represent 20% and one fold deviation, respectively. Error bars are based on the standard deviation of at least three repeats.

that the kinetics of the dissociation reaction were not rate determining.

- The inhibitive effect of acetic acid was explained through its adsorption on the metal surface, which was well defined by a Temkin type adsorption isotherm. Different adsorption constants over the anodic and cathodic current suggested a competitive adsorption scenario depending on the electrode potential and the dominant electron transfer reaction.
- The results reported in the present study suggest that the presence of acetic acid affects the acidic corrosion of mild steel through two mechanisms:
 - Acetic acid increases the corrosion rate through buffering the H^+ concentration at the metal surface, if the corrosion current is under mass transfer control.

- Acetic acid decreases the corrosion rate by inhibiting the charge transfer rates, if the corrosion current is under charge transfer control.
- Elevated temperatures were shown to have a synergistic effect on acetic acid corrosion by shifting the corrosion current towards the mass transfer limiting condition, where acetic acid has a determinant effect.

Acknowledgments

The authors would like to acknowledge the financial support from Anadarko, Baker Hughes, BP, Chevron, CNOOC, ConocoPhillips, DNV GL, ExxonMobil, M-I SWACO (Schlumberger), Multi-Chem (Halliburton), Occidental Oil Company, Petrobras, PTT, Saudi Aramco, Shell Global Solutions, SINOPEC (China Petroleum), TOTAL, and Wood Group Kenny under a joint industrial research project.

Nomenclatures

A	Surface area, m^2
C_i	Concentration of species i , M
C_i^b	Concentration of species i at bulk, M
C_i^s	Concentration of species i at metal surface, M
D_i	Diffusion coefficient of species i , m^2/s
$D_{i,ref}$	Diffusion coefficient of species i at reference temperature, m^2/s
E	Electrode potential, V
E_a	Activation energy, J
E_{0j}	Standard potential of reaction j , V
F	Faradays constant, C/mol
ΔH_j	Enthalpy of reaction j , kJ/mol
i_j	Current density of reaction j , A/m^2
K_j	Equilibrium constant of reaction j
k_{0j}	Rate constant of electrochemical reaction j
$k_{0j,ref}$	Rate constant of electrochemical reaction j at reference temperature
k_f	Forward reaction rate constant
k_b	Backward reaction rate constant
m_i	Reaction order with respect to species i
n_j	Number of transferred electrons in electrochemical reaction j
n_r	Number of reacting species
n_p	Number of produced species
N_i	Flux of species i , $mol/m^2 s$
r	Temkin adsorption isotherm correlation coefficient
R	Universal gas constant, J/K mol
R_i	Reaction rate of species i , M/s
S_{ij}	Stoichiometric coefficient of species i in reaction j
T	temperature, K
T_{ref}	Reference temperature, K
t	Time, s
u_i	Mobility of species i , m/s
v_x	Velocity along x axis, m/s
x	Distance from metal surface, m
Z_i	Charge of ion i
α_j	Transfer coefficient of electrochemical reaction j
δ	Diffusion layer thickness, m
μ	Water viscosity, kg/s.m
μ_{ref}	Water viscosity at reference temperature, kg/s.m
θ	Surface coverage by acetic acid
ρ_w	Density of water, kg/m^3
ν	Kinematic viscosity, m^2/s
ϕ	Electric potential inside liquid, V

ω Angular velocity, rad/s

References

- [1] A. Kahyarian, M. Achour, S. Nesić, CO₂ corrosion of mild steel, in: A.M. El-Sherik (Ed.), Trends Oil Gas Corros. Res. Technol, Elsevier, 2017, pp. 149–190.
- [2] S. Nesić, Key issues related to modelling of internal corrosion of oil and gas pipelines - a review, Corros. Sci. 49 (2007) 4308–4338, <https://doi.org/10.1016/j.corsci.2007.06.006>.
- [3] M.B. Kermani, A. Morshed, Carbon dioxide corrosion in oil and gas production - a compendium, Corrosion 59 (2003) 659–683, <https://doi.org/10.5006/1.3277596>.
- [4] S. Nesić, W. Sun, Corrosion in acid gas solutions, Shreir's Corros. (2010) 1270–1298.
- [5] S. Nesić, Carbon Dioxide Corrosion of Mild Steel, in: Uhlig's Corros. Handb. Third Ed, 2011, pp. 229–245, <https://doi.org/10.1002/9780470872864.ch19>.
- [6] Y.M. Gungalton, Combining research and field data for corrosion rate prediction, CORROSION (1996), Paper No. 27.
- [7] R.R. Garber, James D. Perkins, Richard S. Jangama, Vamishidhar R. Alapati, Calculation of downhole pH and delta pH in the presence of CO₂ and organic acids, CORROSION (1996) 175–200.
- [8] T.I.R. Utvik, Chemical characterization of produced water from four offshore oil production platforms in the north sea, Chemosphere 39 (1999) 2593–2606.
- [9] T. Barth, Organic acids and inorganic ions in waters from petroleum reservoirs, Norwegian continental shelf: a multivariate statistical analysis and comparison with American reservoir formation waters, Appl. Geochem. 6 (1991) 1–15, [https://doi.org/10.1016/0883-2927\(91\)90059-X](https://doi.org/10.1016/0883-2927(91)90059-X).
- [10] J.-L. Crolet, N. Thevenot, A. Dugstad, Role of free acetic acid on the CO₂ corrosion of steels, CORROSION (1999), Paper No. 24.
- [11] P. Menaud, Causative agents of corrosion in distillate field, Oil Gas. J. 43 (1944) 80–81.
- [12] E. Gulbrandsen, K. Bilkova, Solution chemistry effects on corrosion of carbon steels in presence of CO₂ and acetic acid, CORROSION (2006), Paper No. 364.
- [13] K.S. George, S. Nesić, Investigation of carbon dioxide corrosion of mild steel in the presence of acetic acid-part 1: basic mechanisms, Corrosion (2007) 178–186, <https://doi.org/10.5006/1.3278342>.
- [14] P.C. Okafor, B. Brown, S. Nesić, CO₂ corrosion of carbon steel in the presence of acetic acid at higher temperatures, J. Appl. Electrochem 39 (2009) 873–877, <https://doi.org/10.1007/s10800-008-9733-x>.
- [15] Z. Jia, X. Li, C. Du, Z. Liu, J. Gao, Effect of acetic acid on CO₂ corrosion of 3Cr low-alloy steel, Mater. Chem. Phys. 132 (2012) 258–263, <https://doi.org/10.1016/j.matchemphys.2011.08.034>.
- [16] S.D. Zhu, A.Q. Fu, J. Miao, Z.F. Yin, G.S. Zhou, J.F. Wei, Corrosion of N80 carbon steel in oil field formation water containing CO₂ in the absence and presence of acetic acid, Corros. Sci. 53 (2011) 3156–3165, <https://doi.org/10.1016/j.corsci.2011.05.059>.
- [17] J. Amri, E. Gulbrandsen, R.P. Nogueira, Role of acetic acid in CO₂ top of the line corrosion of carbon steel, CORROSION (2011), Paper No. 329.
- [18] T. Tran, B. Brown, S. Nesić, Investigation of the electrochemical mechanisms for acetic acid corrosion of mild steel, Corrosion 70 (2014) 223–229.
- [19] A. Kahyarian, B. Brown, S. Nesić, Mechanism of cathodic reactions in acetic acid corrosion of iron and mild steel, Corrosion 72 (2016) 1539–1546, <https://doi.org/10.5006/2177>.
- [20] A. Kahyarian, M. Achour, S. Nesić, Mathematical modeling of uniform CO₂ corrosion, in: A.M. El-Sherik (Ed.), Trends Oil Gas Corros. Res. Technol, Elsevier, 2017, pp. 805–849.
- [21] A. Kahyarian, M. Singer, S. Nesić, Modeling of uniform CO₂ corrosion of mild steel in gas transportation systems: a review, J. Nat. Gas. Sci. Eng. 29 (2016) 530–549, <https://doi.org/10.1016/j.jngse.2015.12.052>.
- [22] A. Kahyarian, B. Brown, S. Nesić, Mechanism of the hydrogen evolution reaction in mildly acidic environments on gold, J. Electrochem. Soc. 164 (2017) 365–374, <https://doi.org/10.1149/2.1061706jes>.
- [23] J. Newman, K.E. Thomas-Alyea, Electrochemical Systems, 3rd Ed, Wiley-interscience, 2004.
- [24] W.G. Cochran, The flow due to a rotating disc, Math. Proc. Camb. Philos. Soc. 1 (1934) 365–375, <https://doi.org/10.1017/S0305004100012561>.
- [25] J.O. Bockris, D. Drazic, A.R. Despic, The electrode kinetics of the deposition and dissolution of iron, Electrochim. Acta 4 (1961) 325–361, [https://doi.org/10.1016/0013-4686\(62\)87007-8](https://doi.org/10.1016/0013-4686(62)87007-8).
- [26] A.A. El Miligy, D. Geana, W.J. Lorenz, A theoretical treatment of the kinetics of iron dissolution and passivation, Electrochim. Acta 20 (1975) 273–281, [https://doi.org/10.1016/0013-4686\(75\)90005-5](https://doi.org/10.1016/0013-4686(75)90005-5).
- [27] M. Nordsveen, S. Nesić, R. Nyborg, A. Stangeland, A mechanistic model for carbon dioxide corrosion of mild steel in the presence of protective iron carbonate films - part 1: theory and verification, Corrosion 59 (2003) 443–456, <https://doi.org/10.5006/1.3277592>.
- [28] J. Newman, Numerical solution of coupled, ordinary differential equations, Ind. Eng. Chem. Fundam. 7 (1968) 514–517.
- [29] D. Drazic, Iron and its electrochemistry in an active state, Mod. Asp. Electrochem 19 (1989) 62–192.
- [30] S. Nesić, N. Thevenot, J.L. Crolet, D. Drazic, Electrochemical properties of iron dissolution in the presence of CO₂ - basics revisited, CORROSION (1996), Paper No. 03.

- [32] A.J. Bard, L.R. Faulkner, *Electrochemical Methods: Fundamentals and Applications*, John Wiley & Sons, INC, 2001, <https://doi.org/10.1016/j.aca.2010.06.020>.
- [33] N. Pentland, J.O. Bockris, E. Sheldon, Hydrogen evolution reaction on copper, gold, molybdenum, palladium, rhodium, and iron, *J. Electrochem. Soc.* 104 (1957) 182, <https://doi.org/10.1149/1.2428530>.
- [34] J.O. Bockris, J. McBreen, L. Nanis, The hydrogen evolution kinetics and hydrogen entry into α -iron, *J. Electrochem. Soc.* 112 (1965) 1025–1031, <https://doi.org/10.1149/1.2423335>.
- [35] D.M. Dražić, C.S. Hao, The anodic dissolution process on active iron in alkaline solutions, *Electrochim. Acta* 27 (1982) 1409–1415, [https://doi.org/10.1016/0013-4686\(82\)80031-5](https://doi.org/10.1016/0013-4686(82)80031-5).
- [36] M. Keddad, Anodic Dissolution, in: *Corros. Mech. Theory Pract.* Third Ed. CRC Press, 2011, pp. 149–215, <https://doi.org/10.1201/b11020-4>.
- [37] H.S. Harned, R.W. Ehlers, The dissociation constant of acetic acid from 0 to 60° centigrade, *J. Am. Chem. Soc.* 55 (1933) 652–656, <https://doi.org/10.1021/ja01329a027>.
- [38] W.L. Marshall, E.U. Franck, Ion product of water substance, 0–1000 °C, 1–10,000 bars New International Formulation and its background, *J. Phys. Chem. Ref. Data* 10 (1983) 295–304, <https://doi.org/10.1063/1.555643>.
- [39] M. Eigen, E. Eyring, Fast protolytic reactions in aqueous solutions of amino-benzoic acids, *J. Am. Chem. Soc.* 84 (1962) 3254–3256, <https://doi.org/10.1021/ja00876a008>.
- [40] M. Eigen, Proton-transfer, acid-base catalysis, and enzymatic hydrolysis, *Angew. Chem. Int. Ed. Engl.* 3 (1964) 1–72.
- [41] F.H. Stillinger, Proton transfer reactions and kinetics in water, *Theor. Chem. Adv.* 3 (1978) 177–234.
- [42] W.M. Haynes, *CRC Handbook of Chemistry and Physics*, 2009.
- [43] L. Korson, W. Drost-Hansen, F.J. Millero, Viscosity of water at various temperatures, *J. Phys. Chem.* 73 (1969) 34–39, <https://doi.org/10.1021/j100721a006>.
- [44] Y. Zheng, B. Brown, S. Nešić, Electrochemical study and modeling of H₂S corrosion of mild steel, *Corrosion* 70 (2014) 351–365.